A&A manuscript no.
(will be inserted by hand later)

Your thesaurus codes are:
11 (11.09.1; 11.09.2; 11.19.3; 13.09.1)

ASTRONOMY
AND
ASTROPHYSICS
5.9.1996

The starburst galaxy NGC 6090: from 2.5μm to 200μm *

J. A. Acosta-Pulido[1,2,3], **U. Klaas**[1,2], **R. J. Laureijs**[2], **B. Schulz**[2], **U. Kinkel**[1,2], **P. Ábrahám**[1,6], **H. O. Castañeda**[1,2,3], **L. Cornwall**[2,4], **C. Gabriel**[2], **I. Heinrichsen**[2,5], **U. Herbstmeier**[1], **H. Krüger**[1], and **G. Pelz**[1,2]

[1] Max–Planck–Institut für Astronomie, Königstuhl 17, D-69117 Heidelberg, Germany
[2] ISO Science Operations Centre, Astrophysics Division of ESA, VILSPA, Aptdo. Correos 50727, E-28080 Madrid, Spain
[3] Instituto de Astrofísica de Canarias, E-38200 La Laguna, Spain
[4] CLRC, Rutherford Appleton Laboratory, Chilton, Didcot, Oxon, OX11 0QX, UK
[5] Max–Planck–Institut für Kernphysik, Saupferscheckweg 1, D-69117 Heidelberg, Germany
[6] Konkoly Observatory of the Hungarian Academy of Sciences, P.O. Box 67, H-1525 Budapest, Hungary

Received:, Acepted:

Abstract. We have carried out broad band photometry of the interacting galaxy system NGC 6090 from 3.6 to 200 μm using ISOPHOT. This is complemented by a low resolution spectrum in the wavelength range 2.5-11.5 μm. The IR spectral energy distribution of a starburst galaxy is shown with unprecedented detail. From our Far Infrared measurements we can demonstrate that the starburst component is the dominating energy source in this object. 84% of the total IR output is in the wavelength range below 120 μm, while 16% is in the 120 to 240 μm range. Emission in the PAH bands is an essential radiation mechanism in the wavelength range shortward of 10μm for this object. We discuss various published starburst models and their applicability to NGC 6090.

Key words: galaxies individual – NGC 6090 – galaxies starburst – galaxies interactions – infrared galaxies

1. Introduction

NGC 6090 is an entry of the IRAS Bright Galaxy Sample (Soifer et al. 1989), being a luminous galaxy with an IR luminosity larger than $10^{11}L_{\odot}$. IRAS only marginally resolved it at 12 μm and 25 μm.

The galaxy is at a distance of 117 Mpc (we adopt $H_0 = 75 \mathrm{km\,s^{-1} Mpc^{-1}}$ throughout this paper). In the optical NGC 6090 appears as a strongly interacting galaxy system in the process of being merged (see Fig 1). The separation of the two nuclei is 6.4″, corresponding to a projected distance of 3.6 kpc, and they have similar brightness (Mazzarella & Boroson 1993). Optical spectroscopy indicates that both nuclei can be classified as HII region–like (Veilleux et al. 1995).

NGC 6090 has also been observed at 1300 μm (Chini, Krügel, & Kreysa 1992) and in the UV (Kinney et al. 1993). Our study in the 2.5 to 200 μm range complement these previous observations, making it an excellent object for a multiwavelength discussion. In this paper we describe our observations, which include the wavelength region where NGC 6090 is expected to be most luminous.

2. Observations and Data Analysis

Observations were carried out with ISOPHOT (Lemke et al. 1996) using the full wavelength range of this instrument. Raster observations with the ISOPHOT cameras in the 60 μm to 200 μm range (C100 and C200 arrays) were carried out on ISO's 13th revolution. These were effectively a by–product of the testing of the timing of the instrument command sequences. The same sequence of measurements was repeated twice, once from Villafranca ground station and once from Goldstone. Both sequences were performed on the best part of the revolution around apogee. Photometry between 3.6 μm and 60 μm using the 79″aperture (ISOPHOT-P) and Spectroscopy in the range 2.5 μm to 11.6 μm (ISOPHOT-S) were carried out later. The photometer aperture and the coverage of the raster maps relative to an optical image are shown in Fig. 1.

The data were reduced using the ISOPHOT Interactive Analysis. Starting from Edited Raw Data (ERD) level we have corrected for a number of effects in the data: Non–linearity of integration ramps, glitch events, and drift sta-

Send offprint requests to: jacosta@iso.vilspa.esa.es
* Based on observations made with ISO, an ESA project with instruments funded by ESA Member States and with the participation of ISAS and NASA

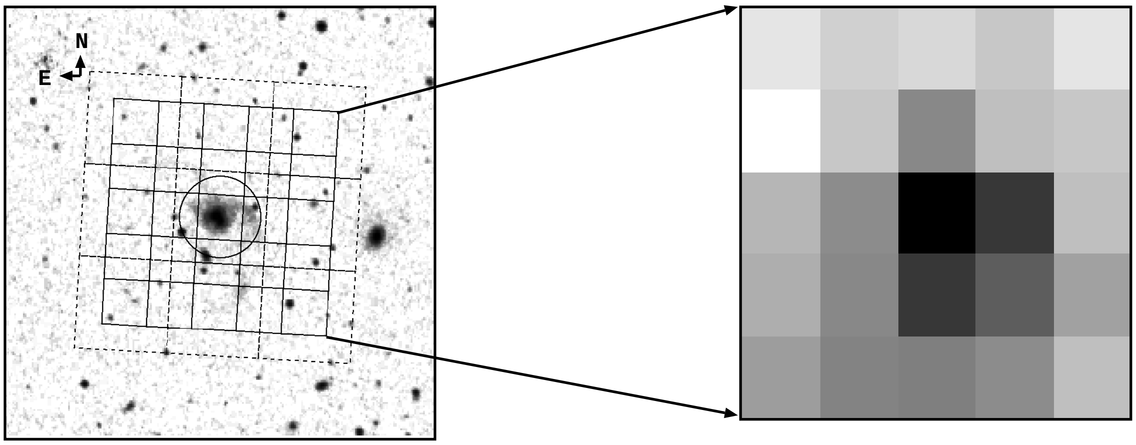

Fig. 1. Left: Overlay of ISOPHOT apertures and raster positions on a POSS image. Solid lines represent C100 pixel positions, dashed lines the C200 pixel positions, and the circle represents the 79$''$aperture. Right: Raster map from the C100 array observation using the 60 μm filter. Same orientation as optical image but not rotated.

bility analysis. For non–chopped measurements we have subtracted the standard dark current. A background subtraction for chopped measurements was done constructing the difference between on and off beams. Fig. 1 shows that our observations detect extended emission at 60 μm, which is consistent with the distribution of objects in our field of view. For C100 rasters we derived the background signal from the edge pixels of the rasters. C200 rasters were not large enough to measure the background signal alone. In this case we disentangled the relative source and background contribution considering the projection of the point spread function onto the individual raster pixels.

2.1. Broad band IR Photometry

The flux calibration was carried out using responsivities for all detectors derived from measurements of several celestial standard sources. Responsivity drift along the orbit was checked using measurements from internal calibrators. We found a variation of less than 10% for our set of measurements. The uncertainty of the responsivity values is around 20-30 %. The total errors are estimated by adding quadratically the measurement error of the signal and the systematic errors in the standard models.

An empirical signal correction needed to be applied to the chopped 11.5 μm and 60 μm measurements presented here to correct for transient behaviour. This is due to the fact that the signal cannot reach a stable value during one chopper plateau period. In order to compare with models we also applied colour corrections to the bandpasses longwards of 60 μm, assuming a blackbody spectrum with a temperature of 35 K.

2.2. Spectrophotometry

The flux calibration of the ISOPHOT-S spectrum was done using the most up-to-date version of the spectral response function for point sources (Lemke et al. 1996). The spectrophotometry is consistent with our broad band photometry in the overlapping bandpasses within a factor $\sim$ 2, the ISOPHOT-P photometry always giving higher fluxes. This can be explained by a beam size effect because the ISOPHOT-S aperture covers only the central part of the galaxy, which is extended with respect to the strongly peaking beam profile of the spectrophotometer.

3. Results

3.1. Spectral Energy Distribution

The Spectral Energy Distribution (SED) is shown in Fig. 2. The shape of the SED is very well constrained by our 14 data points distributed between 3.6 μm and 200 μm. It is clear that most of the energy is emitted in the wavelength range from 60 μm to 120 μm. The C200 photometry clearly shows the SED falling off beyond 120μm. A small bump can be seen in the range 12-16μm. This could not be seen from the IRAS data, but can be seen here due to ISOPHOT's better coverage of this wavelength range.

Our photometry matches that of the IRAS data at 25 μm and 60 μm (Soifer et al. 1989) within the error bars. Our measurement with the 105 μm filter is also in good agreement with the IRAS data point, however the flux measured in the 90 and 100μm filters is too low compared with the IRAS value. Our measured flux in the 11.5 μm filter is higher than that from IRAS measurements. Several strong emission lines (PAH feature at 11.3 μm and [NeII]12.8μm) are present within the wide bandpass of our filter, therefore our assumption of a flat spectrum when converting from in–band power to flux density is probably not valid. Moreover the relative response of the ISOPHOT filter/detector combination is higher at the wavelengths corresponding to these features.

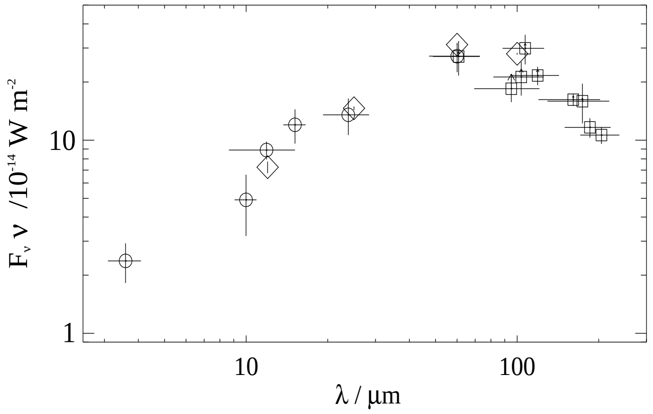

Fig. 2. Spectral energy distribution (νS_ν). Filled circles: ISOPHOT-P apertures measurements; filled squares: ISOPHOT-C measurements; open diamonds: IRAS values. The arrows indicate the applied colour correction.

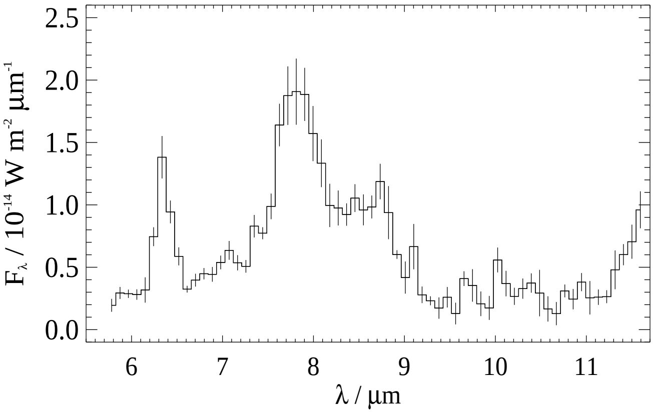

Fig. 3. ISOPHOT-S spectrum of NGC 6090. Only the long wavelength part (5.8–11.6 μm) is shown.

3.1.1. IR Luminosity

We have derived the total infrared luminosity using 11 filters, out of the 14 measured, by constructing non–overlapping bandpasses to cover the whole wavelength range from 3 μm to 240 μm. The total IR luminosity derived for this range is $2.78\times10^{11}\,L_\odot$. For comparison we also calculated the standard IRAS FIR luminosity between 40 μm and 120 μm (Lonsdale et al. 1985), which amounts to 1.39 $\times10^{11}\,L_\odot$, or 50% of the total infrared luminosity. The Extreme FIR luminosity, beyond 120 μm, is 4.5 $\times10^{10}\,L_\odot$, and contributes 16%. The range shortwards of 40 μm gives 9.4 $\times10^{10}L_\odot$, which is 34% of the total IR luminosity. We derive the formation rate of massive stars using an expression given by Scoville & Young (1983) as being $21M_\odot$ year^{-1}. This value is consistent with the one derived from the derredened Hα luminosity given in Veilleux et al. (1995) and using their conversion formula ($17M_\odot$ year^{-1}).

3.2. Emission Lines

The most prominent features in the ISOPHOT-SL (6 – 11.5 μm) spectrum of NGC 6090 (see Fig. 3) are the PAH emission features. We have clearly detected several bands: 6.2, 7.7, 8.6 and 11.3 μm. It is important to notice that due to the redshift the 11.3 μm feature is only partly within our wavelength range. Its flux is calculated assuming that half of the line flux can be measured, which could be underestimated. The short wavelength spectrum (ISOPHOT-SS) is very noisy and we only claim the marginal detection of the 3.3μm PAH feature because of the clear presence of other features at longer wavelengths. We derived the following line intensities: 0.73, 2.5, 7.6, 3.14 and 4.8 (in units of 10^{-15}Wm^{-2}), at rest wavelengths 3.3, 6.2, 7.7, 8.6 and 11.3 μm , respectively. This yields a luminosity in PAH features of at least $8\times10^{9}L_\odot$, which is about 10% of the luminosity between 2 and 40 μm. We cannot confirm the presence of the 9.7μm silicate absorption feature, because of the difficulty to establish the continuum level in–between the bright PAH features.

4. Discussion

A common approach to modelling the infrared emission from galaxies is to assume a mixture of the following 3 components, each with a different heating source (Helou 1986; Rowan–Robinson & Crawford 1989): cold dust or cirrus emission heated by the interstellar radiation field, warm dust associated with star formation regions and hot dust around an active nucleus. These above authors presented the location of various types of galaxies on IRAS colour-colour diagrams, and were able to separate the contribution from the different components. The large S(60)/S(25) ratio for NGC 6090 indicates that the contribution from hot dust heated by an active galactic nucleus is very low. This argument is also corroborated by the presence of PAH features found in our ISOPHOT-S spectrum (Roche et al. 1991; Voit 1992). Furthermore, it does not show any sign of Seyfert activity in the optical (Kim et al. 1995).

Rowan–Robinson & Crawford (1989) and Xu & De Zotti (1989) found the ratio of the starburst emission to the cirrus emission to be 2 to 1. Our result showing that 84% of the emission comes from the wavelength regime shortwards of 120 μm also argues for very efficient heating of the dust. It implies temperatures higher than about 25 K, which cannot be accounted for by the interstellar radiation field alone.

We tried to fit several different model spectra to our photometric data points (see Fig. 4). The model published by Rowan–Robinson & Efstathiou (1993) cannot explain the bump at 16 μm, the PAH features and the continuum shape shortwards of 10 μm. Krügel & Siebenmorgen (1994) proposed a more detailed model, including PAH features, which they applied to the central region of M 82.

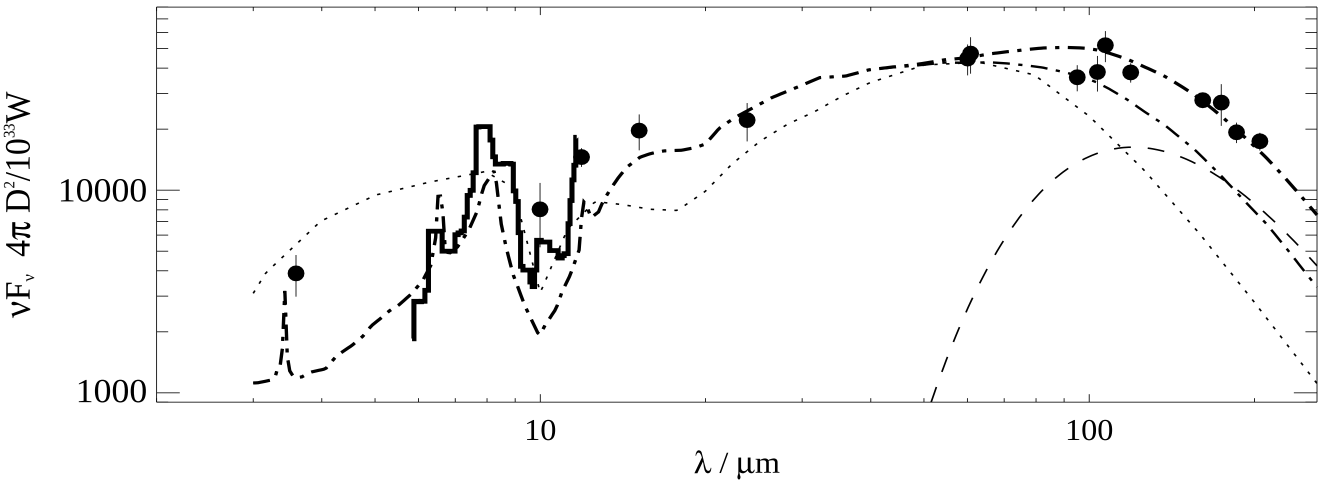

Fig. 4. Model fits to SED of NGC 6090. Filled circles are the measured data points and thick solid line is the ISOPHOT-S spectrum. Dotted line: starburst model from Rowan–Robinson & Efstathiou (1993); Dotted–dashed line: starburst model from Krügel & Siebenmorgen (1994); dashed line: modified blackbody spectrum, and thick dotted–dashed line: the composite of the last two components.

Their predicted SED also shows a bump at around 16 μm. It fits our measured SED very well. Also, our measured PAH line ratios of NGC 6090 are similar to those of M 82 (Léger, d'Hendecourt, & Défourneau 1989).

Neither model accounts for the emission from cold dust beyond 100 μm. To account for this, we added a component with a temperature of around 20 K to the model by Krügel & Siebenmorgen (1994). We assumed a modified blackbody with the shape $\nu^2 B_\nu$, which yields a total luminosity between 3 and 1300 μm of $4.4 \times 10^{10} L_\odot$. The 1300 μm point given by Chini, Krügel, & Kreysa (1992) cannot be used as an additional confinement for the model fits because it samples only the very central region of the system (11″). Using the conversion formula given in Chini, Krügel, & Kreysa (1992), we derived a dust mass of $10^8 M_\odot$ for this component. This is very likely to be close to the total dust mass of the galaxy. If we assume an average dust temperature of the starburst component of 50 K, we derive that the dust mass involved in this emission is $10^6 M_\odot$, which is approximately 1% of the previously derived total dust mass.

5. Conclusions

The IR emission of NGC 6090 is dominated by warm dust heated by young stars forming in the merging process. A model by Krügel & Siebenmorgen (1994) complemented by a cold dust component of $T \simeq 20$K and a mass of 10^8 $M_\odot$ describes its properties very well. NGC 6090 shows a SED similar to M 82, although it is more than 10 times brighter and its starburst region may be considerably larger. For wavelengths shorter than 20μm, the contribution made by PAH molecules to the total emission is significant.

Acknowledgements. We are grateful to all people at the ground station in Vilspa. We acknowledge the work of the whole ISOPHOT team in building the instrument. ISOPHOT was funded by the Deutsche Agentur für Raumfahrtangelegenheiten (DARA), the Max Planck Society and several European institutes.

References

Chini R., Krügel E., Kreysa E., 1992, A&A, 266, 177
Helou G., 1986, ApJ, 311, L33
Kim D.-C., Sanders D. B., Veilleux S., Mazzarella J. M., Soifer B. T., 1995, ApJS, 98, 129
Kinney A. L., Bohlin R. C., Calzetti D., Panagia N., Wyse R. F. G., 1993, ApJS, 86, 5
Krügel E., Siebenmorgen R., 1994, A&A, 282, 407
Léger A., d'Hendecourt L., Défourneau D., 1989, A&A, 216, 148
Lemke D., Klaas U., Abolins J., et al., 1996, A&A this volume
Lonsdale C., Helou G., Good J. C., Rice W. L., 1985, Cataloged Galaxies and Quasars Observed in the IRAS survey
Mazzarella J. M., Boroson T. A., 1993, AJ, 85, 27
Roche P. F., Aitken D. K., Smith C. H., Ward M. J., 1991, MNRAS, 248, 606
Rowan–Robinson M., Crawford J., 1989, MNRAS, 238, 523
Rowan–Robinson M., Efstathiou A., 1993, MNRAS, 263, 675
Scoville N., Young J. S., 1983, ApJ, 256, 148
Soifer B. T., Boehmer L., Neugebauer G., Sanders D. B., 1989, AJ, 98, 766
Veilleux S., Kim D.-C., Sanders D. B., Mazzarella J. M., Soifer B. T., 1995, ApJS, 98, 171
Voit G. M., 1992, MNRAS, 258, 841
Xu C., De Zotti G., 1989, A&A, 225, 12

This article was processed by the author using Springer-Verlag LaTeX A&A style file *L-AA* version 3.